Mechanical characterisation of a structural battery electrolyte

Downloaded from: https://research.chalmers.se, 2026-09-09 13:09 UTC

Citation for the original published paper (version of record):
Tavano, R., Spagnol, M., Al-Ramanhi, N. et al (2024). Mechanical characterisation of a structural battery electrolyte. Polymer, 312. http://dx.doi.org/10.1016/j.polymer.2024.127646

N.B. When citing this work, cite the original published paper.

research.chalmers.se offers the possibility of retrieving research publications produced at Chalmers University of Technology. It covers all kind of research output: articles, dissertations, conference papers, reports etc. since 2004. research.chalmers.se is administrated and maintained by Chalmers Library

(article starts on next page)

Polymer 312 (2024) 127646

Contents lists available at ScienceDirect

Polymer

journal homepage: www.elsevier.com/locate/polymer

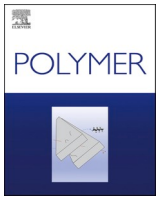

Mechanical characterisation of a structural battery electrolyte

Ruben Tavano [a,*], Michele Spagnol [a,b], Nawres Al-Ramahi [c,d], Roberts Joffe [c], Johanna Xu [a], Leif E. Asp [a,**]

[a] Industrial and Materials Science, Chalmers University of Technology, 41258, Göteborg, Sweden
[b] Tecnica e Gestione dei Sistemi Industriali, Universitá degli Studi di Padova, 36100, Vicenza, Italy
[c] Engineering Sciences and Mathematics, Luleå University of Technology, 97187, Luleå, Sweden
[d] Institute of Technology, Middle Technical University, Baghdad, Iraq

ARTICLE INFO

Keywords:
Multifunctionality
Mechanical characterisation
Structural battery electrolyte

ABSTRACT

Structural battery composites require a structural electrolyte to work. The structural battery electrolyte has a bicontinuous microstructure which enables its dual roles: mechanical load transfer and ion transport between the electrodes. These structural electrolytes are difficult to characterise mechanically via bulk tests. For this reason, no extensive characterisation of the mechanical properties of the structural battery electrolyte has been performed to date. In this study, we highlight the many challenges of these types of tests, including the complexity of sample manufacturing, preparation and testing. We further demonstrate a method to prepare test samples and to perform mechanical tests on the structural battery electrolyte. The executed test campaign provides measures of Young's modulus (approximately 412 MPa) and Poisson's ratio (0.34), as well as tensile (4.85 MPa) and compressive strength (32.66 MPa) and strain to failure (2.49 % and 28.11 % in tension and compression, respectively). In addition, cure shrinkage is investigated and found insignificant. These results are crucial for the further development of structural battery composites as they allow for accurate prediction of their internal stress states.

1. Introduction

Multifunctional materials will play a key role in future energy storage. One such multifunctional material is the structural battery composite (SBC), which acts as a composite structural material that simultaneously stores electric energy as a lithium-ion battery [1–4]. The application of structural battery technology is particularly promising within the transport industry. Utilisation of SBCs in load-bearing structures, such as vehicle body panels, and aircraft interiors can lead to substantial mass savings across transport modes. This will enhance fuel efficiency, consequently lowering emissions.

As conventional composite laminates, the SBC consists of a stack of plies to form a laminate. The two outermost plies are the two electrodes: the positive electrode is made of carbon fibres coated with lithium iron phosphate ($LiFePO_4$ or LFP) [5–7] and the negative electrode consists of neat carbon fibre [8–13]. The LFP particles act as the electrochemically active material in the positive electrode (like in conventional lithium-ion batteries) while the carbon fibres act as reinforcement and current collector in the positive electrode. In the negative electrode, the carbon fibres act as active material, similarly to graphite in conventional lithium-ion batteries, as well as reinforcement and current collector. The two electrodes are separated by a thin electrically insulating, ionically conductive, material. The laminated structure is impregnated with a structural battery electrolyte (SBE). The SBE provides load transfer between constituents and enables lithium-ion migration between the electrodes. Thus, an SBE with high combined ionic conductivity and mechanical properties is desired.

The first attempts in SBC electrolytes considered homogeneous liquid electrolyte systems [14]. Very high ionic conductivity was obtained but no mechanical load transfer was achieved. In order to achieve mechanical performance with maintained ionic conductivity, gel polymer electrolyte (GPE) and solid polymer electrolyte (SPE) homogenous soft materials were investigated [15]. However, in general, highly ionic conductive GPEs demonstrated low mechanical properties, while when improved mechanical performances were measured as in SPEs, the ionic conductivity was low [16–20]. To overcome the limitations of

* Corresponding author.
** Corresponding author.
E-mail address: ruben.tavano@chalmers.se (R. Tavano).

https://doi.org/10.1016/j.polymer.2024.127646
Received 25 April 2024; Received in revised form 17 September 2024; Accepted 20 September 2024
Available online 21 September 2024
0032-3861/© 2024 The Author(s). Published by Elsevier Ltd. This is an open access article under the CC BY license (http://creativecommons.org/licenses/by/4.0/).

homogeneous materials in multifunctional applications, heterogeneous electrolyte systems were studied. In these systems, two or more materials are combined to create two or more bicontinuous phases. In this way, a liquid electrolyte (with high ionic conductivity) can be contained within a solid glassy polymer (with high elastic modulus) leading to a much-improved multifunctional performance [21–23]. By this approach commercial liquid electrolytes or ionic liquids can be used together with epoxy or vinyl ester polymers to realise a highly ionic conductive stiff SBE [24–27]. The basis for the currently used heterogeneous SBEs was proposed by Ihrner et al. [28] They mixed an organic electrolyte with dissolved lithium salts and a methacrylate-based monomer to synthesise an SBE via a polymerisation-induced phase separation (PIPS) reaction initiated by UV irradiation. With this approach highly multifunctional SBEs were obtained. The use of UV-induced polymerisation, however, poses manufacturing issues in SBCs due to the non-transparent nature of the materials used in the various constituents. For this reason, thermal curing is a more suitable method for the SBE manufacturing process. Schneider et al. evaluated thermal curing for the same SBE used by Ihrner and assessed the effect of the curing temperature on the curing performance, morphology, ionic conductivity and mechanical performance [29]. Higher curing temperatures were linked to higher conversion rates and shorter curing times. Similar morphologies were obtained for all the curing temperatures. No significant effect of the curing temperature was identified on the ionic conductivity and the mechanical behaviour.

To achieve a better understanding of the SBE Cattaruzza et al. [30] investigated porosity and the liquid electrolyte uptake in the glassy polymeric phase and measured the ionic conductivity of various liquid electrolyte to monomer mixture ratios. The ionic conductivity of the SBE was $2.9{\cdot}10^{-4}$ S cm^{-1}, which is merely 10 % of that of the liquid electrolyte (a 1 M solution of lithium bis(trifluoromethanesulfonyl)imide (LiTFSI) salt, in an organic solvent mixture, ethylene carbonate and propolene carbonate (EC:PC)). The most promising SBE composition identified was further studied by Duan et al. who made a 3D reconstruction of the SBE [31]. They generated a series of 2D images via scanning electron microscopy (SEM) following ion milling of 20 nm thick layers of material. These images were then utilised to build a 3D model which was used to determine the tortuosity, average pore size, and to estimate the elastic modulus and the ionic conductivity using finite element analysis.

Knowledge about the structure of the SBE and its electro-chemo-mechanical properties is needed to model the SBE and its behaviour in SBCs. This is particularly evident considering the extensive volume changes that occur in the carbon fibres and the LFP particles during electrochemical cycling. Changes in carbon fibre volume and mechanical properties with state-of-lithiation and the consequence of these changes on the negative structural electrode have been investigated in detail [32–34]. Larsson et al. analysed the internal stress distribution in the SBE from a 6.6 % radial expansion of the carbon fibres for a representative volume element of the negative electrode, showing high stresses in the SBE constrained between carbon fibres [35]. This demonstrates the importance of reliable mechanical data for the composite material constituents for accurate stress predictions. To date, the mechanical properties of the SBE have only been measured using dynamic mechanical analysis (DMA). With DMA, only the storage modulus E′ and loss modulus E″ can be measured. Thus, both the Young's modulus and Poisson's ratio for the SBE remain to be measured. Furthermore, there is a general lack of data describing the behaviour of the SBE material under compression load. Such data are needed for reliable computational analysis of the SBCs. Finally, cure shrinkage of the matrix material will affect the internal stress distribution. However, to the authors' knowledge, no attempt to measure the cure shrinkage during the PIPS reaction of the SBE has yet been made.

In the current study, we fill these gaps by performing a thorough mechanical characterisation of a state-of-the-art SBE. In addition, the cure shrinkage resulting from the PIPS reaction is assessed. The composition of the SBE closely resembles that of previous works by Cattaruzza et al. [30], Larsson et al. [34], and Asp et al. [35], employing identical monomer, solvent, and solid-to-liquid weight ratio in the SBE.

2. Materials and methods

2.1. Materials

The liquid electrolyte was made from a solution of lithium bis(oxalate)borate (LiBOB) and lithium tri(fluoro)methanesulfonate (LiTFS) (with 0.4 M and 0.6 M concentrations respectively) dissolved in a mixture of ethylene carbonate (EC) and propylene carbonate (PC) with a 1:1 weight ratio. The monomer consisted of bisphenol-A ethoxylate dimethacrylate (BPAMA) (M_n: 540 g mol^{-1}) mixed with the thermal initiator 2,2′-azobis(2-methylpropionitrile) (AIBN). A 1 % weight relative to the monomer of the thermal initiator was used. EC, PC, the two lithium salts (LiBOB and LiTFS), the monomer (BPAMA), and the thermal initiator (AIBN) were purchased from Sigma-Aldrich. The SBE was synthesized from a solution consisting of a 50:50 weight ratio of liquid electrolyte and monomer. All the materials were stored inside a glovebox to ensure no moisture and oxygen exposure. All the materials were used as received.

For the tensile test sample preparation, glass sheets and a multi-layer PET/Al/PE film acting as a pouch bag were used. For the compression test sample preparation, 5 mL polypropylene (PP) syringes with 10 mm diameter purchased from Fisher Scientific were used. For the shrinkage test, borosilicate glass tubes with a 4 mm diameter were used. An adhesive rubber was also used to seal the syringes and the borosilicate glass tube.

2.2. Methods

2.2.1. Sample manufacturing

The bulk properties of SBE have previously not been characterised due to the challenges of the manufacturing process. In particular, the polymerisation of BPAMA is terminated by the presence of oxygen. For this reason, the first steps of the sample preparation were conducted inside of a glovebox under a dry argon atmosphere (less than 1 ppm of H_2O and O_2). The lithium salts (LiBOB and LiTFS) were added to the EC:PC solvent mixture. An equal mass of monomer BPAMA was then added to the solution. Furthermore, thermal initiator AIBN was added. All the species were mixed using a vortex mixer until a homogeneous solution was obtained. To avoid entrapped gas in the mixture the container was then left without the lid for 30 minutes.

To manufacture the tensile test samples the obtained mixture was poured inside 10 × 13 cm custom-built glass moulds until the desired thickness of 3 mm was reached. The moulds were then sealed inside a pouch bag to prevent any contact with ambient atmosphere before and during cure. To manufacture the compression test samples, the mixture was drawn with syringes until an approximate 2:1 ratio of length to diameter of the mixture inside the syringe was reached. Approximately 10 mm of free space was left between the tip of the syringe and the mixture to allow any gas developed during the curing process to escape the SBE. The tip of the syringes was sealed using an adhesive rubber. This was done to ensure that the solution was not exposed to oxygen or moisture that could affect the curing process. The mixture content levels in the syringe were marked to allow evaluation of cure shrinkage.

The prepared and sealed tensile and compression samples were cured in an oven outside the glovebox at 90 °C for 1 hour. Images from the various steps of the manufacturing are presented in Fig. S1.

Post cure the obtained SBE slabs were extracted from the moulds and machined with a waterjet cutter into the final dog-bone shape of the tensile test specimens. The SBE cylinders obtained in the syringes were extracted and the ends were machined using a waterjet cutter, resulting in compression test specimens with flat and parallel ends. Images of finished tensile and compression test specimens are presented in Fig. 1a

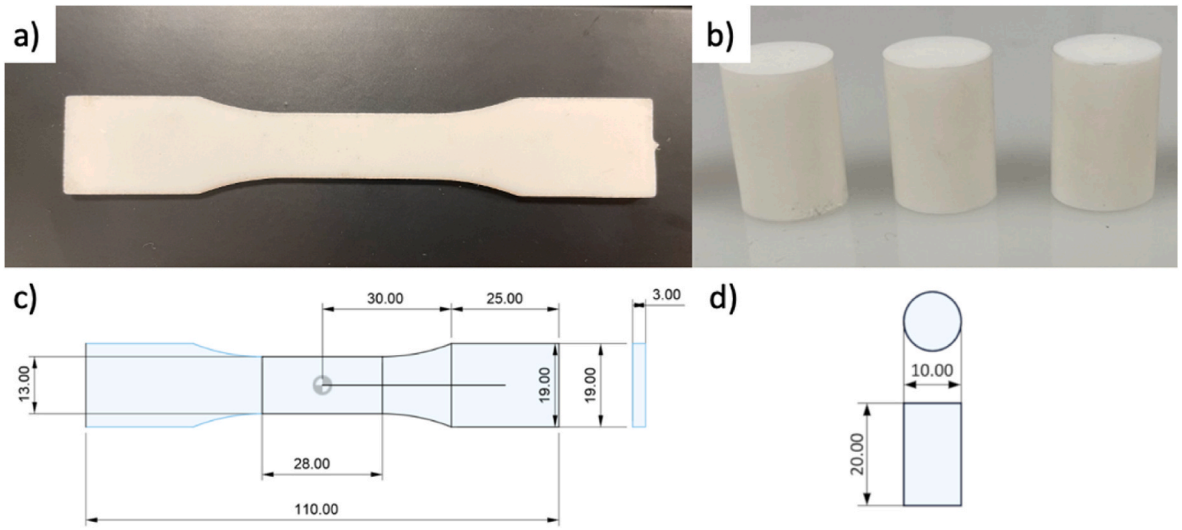

Fig. 1. (a) Tensile dog-bone shaped samples and (b) compression cylindrical sample. Dimensions of (c) tensile test specimens and (d) compression test specimens (all units are expressed in millimetres).

and b. The detailed dimensions of the samples are provided in Fig. 1c and d. Even though a significant part of the material consists of liquid electrolyte, the samples appear dry. This is probably due to the delicate interconnected pore structure which makes liquid electrolyte evaporation from the bulk of the SBE a slow process.

Immediately after machining, the test specimens were sealed inside pouch bags to avoid any liquid electrolyte evaporation and to guarantee that the tested material was the same bi-continuous SBE as that used in the SBCs.

2.2.2. Microscopy

The SBE microstructure was evaluated via SEM imaging using a Zeiss FEGSEM LEO-1550 with an accelerating voltage of 5 kV. Samples were obtained from 3 mm thick SBE pieces fracturing them manually so that the cross-section would not be affected by any cutting tool. The obtained samples were washed in water for two days and dried for one day prior to SEM analyses to remove the liquid electrolyte from the SBE. Finally, samples were sputtered with gold to avoid any charging effects during imaging.

2.2.3. Mechanical tests

Mechanical tests followed the ASTM D638 type IV standard for tension and the ASTM D695 standard for compression. The obtained samples were tested at Luleå University of Technology (Sweden) using an Instron 3366 testing machine with a 10 kN load cell. A fine speckle pattern was applied to the surface of the dog-bone-shaped samples to measure displacements and evaluate the strain by means of digital image correlation technique (DIC) [36]. This was done using matte white paint sprayed on one of the sides of the samples and subsequently, spraying a small amount of black paint to create a random pattern. The images during the loading were recorded using a JAI GO-5000M-USB optical camera positioned perpendicularly to the speckled surface of the sample and centered at the initial centre point of the sample surface.

The parameters for the used DIC setup are summarised in Table 1.

The Zeiss Inspect software was used to create a fictitious extensometer on the speckle pattern and follow its evolution during the loading.

Table 1
Parameters used for the DIC setup.

Image resolution [pixels]	Step size [pixels]	Speckle size [pixels]	Stand-off distance [mm]	Subset size [pixels]
2560x1536	5	4–5	400	19x19

The images were processed using a full-field Green-Lagrange strain tensor. A frame was captured every 200 ms and a strain rate of 0.5 mm min^{-1} corresponding to the cross-head displacement speed was used in all tensile tests. This strain rate, although lower than ASTM standards, was intentionally chosen to enhance data resolution and provide better control throughout the test. In total, six tensile specimens were tested.

The tensile samples were first subjected to a loading up to a strain of approximately 0.25 % followed by an unloading to the initial state. This was done to measure Young's modulus and Poisson's ratio of the SBE in the linear-elastic region of the material response during unloading. To obtain the Poisson's ratio, the strain in the longitudinal direction was plotted against the strain in the transverse direction, and the value of the Poisson's ratio was obtained as the slope of the plot. After the initial loading/unloading step the samples were tested with increasing load until failure.

For the cylindrical compression specimens, flat parallel plates were used to apply the load on the two bases of the cylinders. Compression tests were performed at a strain rate of 1 mm min^{-1}. Strain in the compression test was extracted from the top cross-head displacement since the applied speckle pattern was dissolved by the liquid electrolyte seepage at high strain levels. Additionally, the curved surface created numerous reflections, which were captured as visual artefacts by the single optical camera in the current setup. In total, five specimens were tested in compression.

3. Results

3.1. Material structure

The infusion technique used to manufacture state-of-the-art structural battery composites [37] could not be used to manufacture bulk samples of the SBE. Therefore, the co-continuous microstructure of the synthesised bulk SBE test samples was characterised and compared with that of the SBE in SBCs [29–31]. SEM images taken at 10k, 20k, and 50k magnification are presented in Fig. 2. The presence of pores with a wide size distribution is clear already from the lower magnification micrograph. From the image with the highest magnification, it is evident that most of the microstructural features are in the hundreds of nanometres range. This corresponds well with what was previously reported by Duan et al. [31] Tortuosity can only be hypothesised in this case as no ion milling was used to assess the bulk microstructure. However, the similarities to micrographs presented by Duan et al. suggest that the internal porosity and its interconnection are the same.

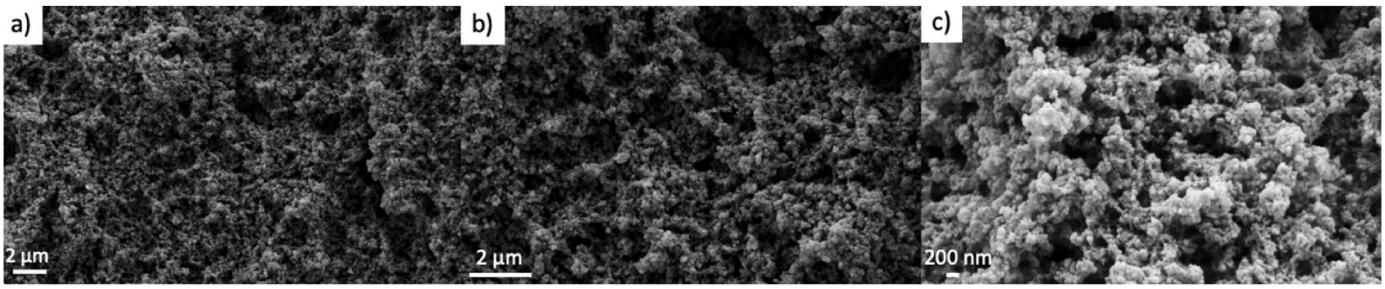

Fig. 2. SEM images of the SBE microstructure at a fracture surface at (a) x10k magnification, (b) x20k magnification, and (c) x50k magnification.

3.2. Cure shrinkage

The levels of the solution in the borosilicate glass tube were marked so that the cure shrinkage could be monitored. After curing, no shrinkage could be identified in the cylinders, as no difference in the height of the solution and the cured SBE could be observed. Furthermore, the sample was very difficult to extract from the tube indicating that no cross-sectional shrinkage took place. If we assume that no radius change takes place, and we consider a typical 7–10 % cure shrinkage for vinyl ester resins, shrinkage should be readily detectable [38]. For a 10 % cure shrinkage, and a constant cross-section area, a reduction in height of approximately 5.5 mm would result. Images of samples before and after curing are presented in Fig. 3a and b.

3.3. Mechanical test results

A typical tensile curve for the SBE samples is presented in Fig. 4a. It is clear that after an initial linearly elastic region at small strains, the behaviour of the material becomes non-linear. In tension, failure occurs at relatively low stresses and strains. An average strength of 4.85 MPa and an average strain to failure of 2.49 % were measured. The brittle nature of the SBE is also visible in the fractured specimens depicted in Fig. 4b and c.

A non-linear stress-strain behaviour of the SBE was also found for compression load as shown in Fig. 5a. For compression load, significantly higher strength and strain to failure were measured. An average compressive strength of 32.7 MPa and an average strain to failure of 28.1 % are observed. A very consistent behaviour was found for the SBE when loaded in compression, reflected by the low scatter in data reported in Table 2. Superior properties in compression are expected since the yield stress of polymer materials is known to be pressure-dependent [39]. However, the compressive yield strength is almost one order of magnitude higher than in tension, compared to conventional thermoset resins where the compressive yield strength is usually two to three times higher than that in tension [40]. This behaviour, observed for other polymeric foams is also characteristic of conventional ceramic materials characterised by a high amount of internal porosity [17,41]. It should be noted that no tests could be performed on the neat polymer material as void-free test samples could not be manufactured. Voids occurred from massive gassing during cure of the neat resin and these gas bubbles remained trapped due to the high viscosity of BPAMA.

As mentioned in the experimental section, speckle patterns could not be used due to the squeeze out of the liquid electrolyte during the compression tests. The liquid electrolyte squeezed out from the cylindrical samples during a test is visible in Fig. 5b. Furthermore, barreling of the test specimen at the end of the compression test is illustrated in Fig. 5c. The specimen split in the centre causing failure.

An overview of the obtained mechanical properties for the SBE is presented in Table 2.

It should be noted that the measured Young's modulus is significantly lower than the storage modulus E′ obtained from DMA measurements, which was reported to be 611 MPa [29].

The tension and compression stress-strain plots from all samples are shown in Fig. 6. The repeatability of the tests is evident.

4. Conclusion

The current study provides a deepened understanding of the

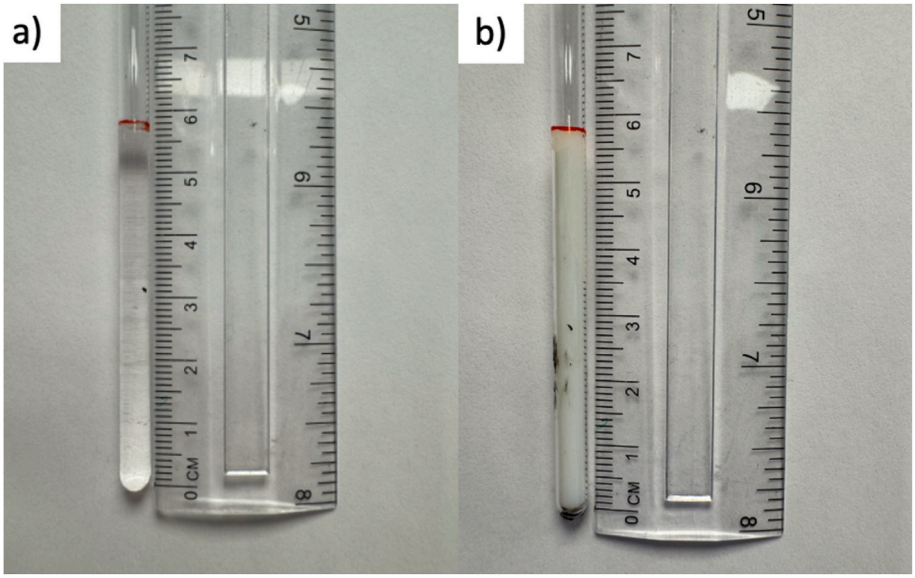

Fig. 3. Curing shrinkage evaluation. (a) Before curing, (b) after curing.

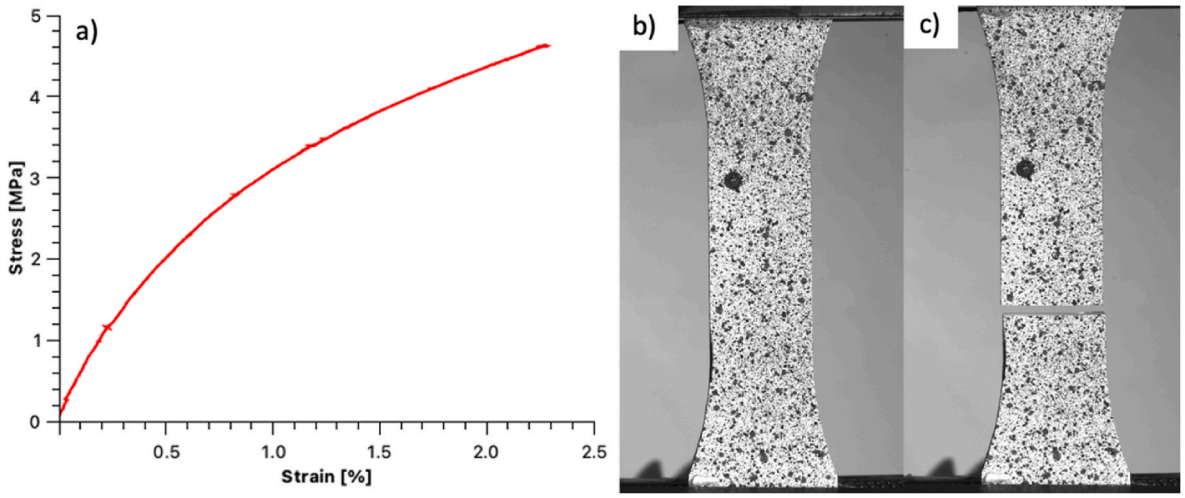

Fig. 4. (a) Typical tensile curve of the SBE dog-bone-shaped specimen. (b) Dog-bone-shaped tensile samples with DIC speckle pattern before and (c) after the testing procedure.

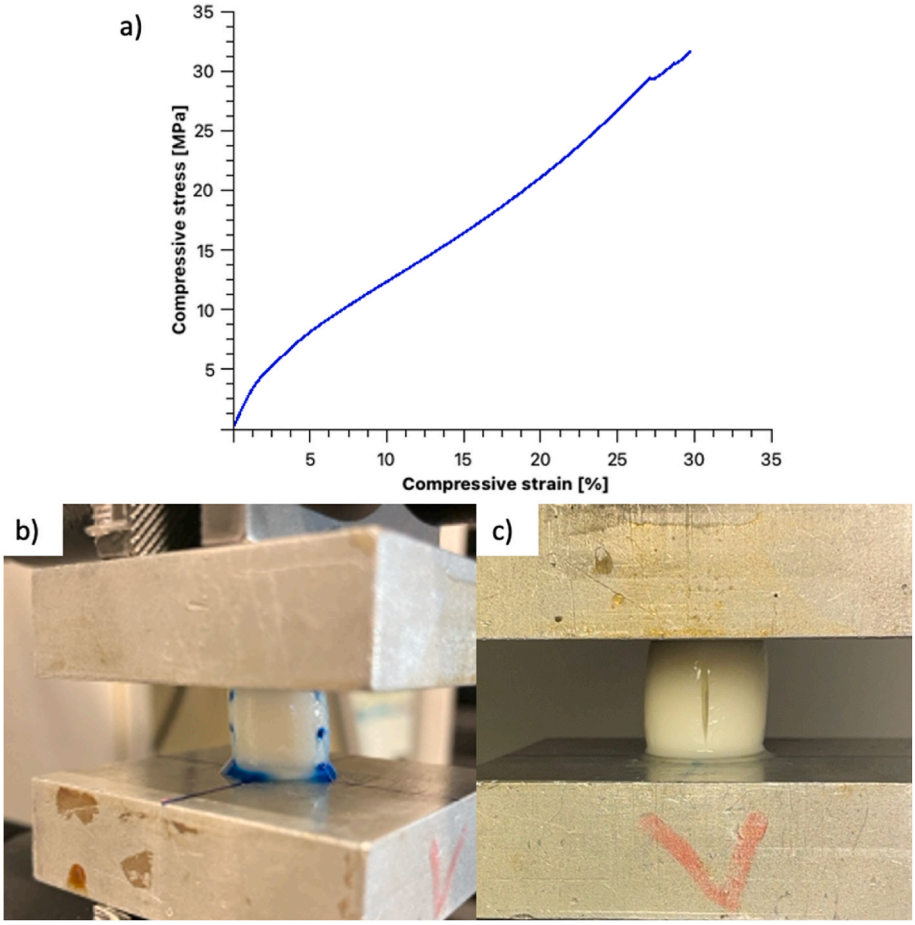

Fig. 5. (a) Typical compression curve of the SBE cylindrical samples. (b) Compression cylinder sample with liquid electrolyte leakage from the bulk of the material. (c) Barreling and cracking of the cylindrical compression samples at the end of the testing procedure.

Table 2
Average material parameters obtained for the tested SBE samples.

Young's modulus [MPa]	Poisson's ratio [−]	Tensile strength [MPa]	Strain to failure (tension) [%]	Compressive strength [MPa]	Strain to failure (compression) [%]
412.47 ± 58.3	0.34 ± 0.04	4.85 ± 0.66	2.49 ± 0.36	32.66 ± 0.63	28.11 ± 0.57

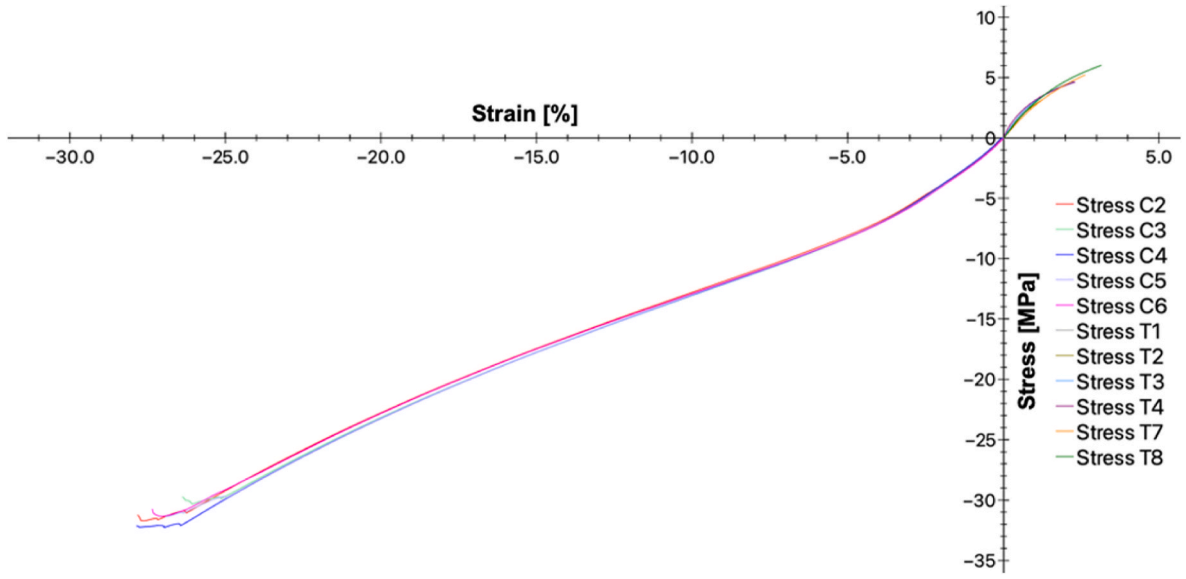

Fig. 6. Comprehensive tensile and compressive curves for the SBE samples.

mechanical behaviour of the structural battery electrolyte. Tests on the bulk material have not previously been performed. Here, a procedure to repeatably and consistently manufacture specimens for mechanical characterisation of bi-phasic structural battery electrolytes is demonstrated. Tensile tests are performed to measure Young's modulus and Poisson's ratio of a bulk structural battery electrolyte. Also, the strength and strain to failure in tension and compression are characterised. In addition, cure shrinkage is monitored and found to be insignificant.

The mechanical characterisation shows a brittle behaviour with a low tensile strength of only 4.85 MPa and a reasonable compressive strength of more than 30 MPa. The measured average Young's modulus of the bicontinuous structural battery electrolyte (412 MPa) is lower compared to neat thermoset polymers and also lower than the storage modulus previously measured by DMA. Finally, a Poisson's ratio of 0.34 was measured.

Equipped with this information, reliable analyses of the internal stress distribution in the structural battery composite at arbitrary state-of-charge and in-service mechanical loading can be performed.

CRediT authorship contribution statement

Ruben Tavano: Writing – original draft, Methodology, Investigation, Formal analysis, Conceptualization. **Michele Spagnol:** Writing – original draft, Methodology, Investigation, Formal analysis. **Nawres Al-Ramahi:** Writing – review & editing, Investigation, Data curation. **Roberts Joffe:** Writing – review & editing. **Johanna Xu:** Writing – review & editing, Supervision, Methodology, Conceptualization. **Leif E. Asp:** Writing – original draft, Supervision, Methodology, Funding acquisition.

Declaration of competing interest

The authors declare that they have no known competing financial interests or personal relationships that could have appeared to influence the work reported in this paper.

Data availability

Data will be made available on request.

Acknowledgements

Funding from ONR (USA) Award No. N62909-22-1-2037, 2D TECH VINNOVA competence Center (Ref. 2019-00068), and USAF (USA) EOARD Award No. FA8655-21-1-7038 is gratefully acknowledged.

Appendix A. Supplementary data

Supplementary data to this article can be found online at https://doi.org/10.1016/j.polymer.2024.127646.

References

[1] L.E. Asp, M. Johansson, G. Lindbergh, J. Xu, D. Zenkert, Structural battery composites: a review, Funct. Compos. Struct. 1 (4) (2019) 042001, https://doi.org/10.1088/2631-6331/ab5571.
[2] L.E. Asp, E.S. Greenhalgh, Structural power composites, Compos. Sci. Technol. 101 (2014) 41–61, https://doi.org/10.1016/j.compscitech.2014.06.020.
[3] L.E. Asp, E.S. Greenhalgh, Multifunctional structural battery and supercapacitor composites, in: Multifunctionality of Polymer Composites, Elsevier, 2015, pp. 619–661, https://doi.org/10.1016/B978-0-323-26434-1.00020-9.
[4] D. Zenkert, R. Harnden, L.E. Asp, G. Lindbergh, M. Johansson, Multifunctional carbon fibre composites using electrochemistry, Compos. B Eng. 273 (2024) 111240, https://doi.org/10.1016/j.compositesb.2024.111240.
[5] J. Hagberg, H.A. Maples, K.S.P. Alvim, J. Xu, W. Johannisson, A. Bismarck, D. Zenkert, G. Lindbergh, Lithium iron phosphate coated carbon fiber electrodes for structural lithium ion batteries, Compos. Sci. Technol. 162 (2018) 235–243, https://doi.org/10.1016/j.compscitech.2018.04.041.
[6] J.S. Sanchez, J. Xu, Z. Xia, J. Sun, L.E. Asp, V. Palermo, Electrophoretic coating of LiFePO4/graphene oxide on carbon fibers as cathode electrodes for structural lithium ion batteries, Compos. Sci. Technol. 208 (2021) 108768, https://doi.org/10.1016/j.compscitech.2021.108768.
[7] Z. Xia, Z. Li, J. Xu, S. Sasidharan, J.S. Sanchez, V. Palermo, L.E. Asp, Green synthesis of positive electrodes for high performance structural batteries - a study on graphene additives, Compos. Sci. Technol. 251 (2024) 110568, https://doi.org/10.1016/j.compscitech.2024.110568.
[8] J. Hagberg, S. Leijonmarck, G. Lindbergh, High precision coulometry of commercial PAN-based carbon fibers as electrodes in structural batteries, J. Electrochem. Soc. 163 (8) (2016) A1790, https://doi.org/10.1149/2.0041609jes.
[9] G. Fredi, S. Jeschke, A. Boulaoued, J. Wallenstein, M. Rashidi, F. Liu, R. Harnden, D. Zenkert, J. Hagberg, G. Lindbergh, P. Johansson, L. Stievano, L.E. Asp, Graphitic microstructure and performance of carbon fibre Li-ion structural battery electrodes, Multifunct. Mater 1 (1) (2018) 015003, https://doi.org/10.1088/2399-7532/aab707.
[10] M. Johansen, C. Schlueter, P.L. Tam, L.E. Asp, F. Liu, Mapping nitrogen heteroatoms in carbon fibres using atom probe tomography and photoelectron spectroscopy, Carbon 179 (2021) 20–27, https://doi.org/10.1016/j.carbon.2021.03.061.

[11] M. Johansen, J. Xu, P.L. Tam, L.E. Asp, F. Liu, Lithiated carbon fibres for structural batteries characterised with auger electron spectroscopy, Appl. Surf. Sci. 627 (2023) 157323, https://doi.org/10.1016/j.apsusc.2023.157323.
[12] M.H. Kjell, E. Jacques, D. Zenkert, M. Behm, G. Lindbergh, PAN-based carbon fiber negative electrodes for structural lithium-ion batteries, J. Electrochem. Soc. 158 (12) (2011) A1455, https://doi.org/10.1149/2.053112jes.
[13] M.H. Kjell, T.G. Zavalis, M. Behm, G. Lindbergh, Electrochemical characterization of lithium intercalation processes of PAN-based carbon fibers in a microelectrode system, J. Electrochem. Soc. 160 (9) (2013) A1473, https://doi.org/10.1149/2.054309jes.
[14] K. Xu, Nonaqueous liquid electrolytes for lithium-based rechargeable batteries, Chem. Rev. 104 (10) (2004) 4303–4418, https://doi.org/10.1021/cr030203g.
[15] J.W. Fergus, Ceramic and polymeric solid electrolytes for lithium-ion batteries, J. Power Sources 195 (15) (2010) 4554–4569, https://doi.org/10.1016/j.jpowsour.2010.01.076.
[16] Y. Wang, W.-H. Zhong, Development of electrolytes towards achieving safe and high-performance energy-storage devices: a review, Chemelectrochem 2 (1) (2015) 22–36, https://doi.org/10.1002/celc.201402277.
[17] A. Manuel Stephan, Review on gel polymer electrolytes for lithium batteries, Eur. Polym. J. 42 (1) (2006) 21–42, https://doi.org/10.1016/j.eurpolymj.2005.09.017.
[18] M. Willgert, M.H. Kjell, E. Jacques, M. Behm, G. Lindbergh, M. Johansson, Photoinduced free radical polymerization of thermoset lithium battery electrolytes, Eur. Polym. J. 47 (12) (2011) 2372–2378, https://doi.org/10.1016/j.eurpolymj.2011.09.018.
[19] N. Ihrner, M. Johansson, Improved performance of solid polymer electrolytes for structural batteries utilizing plasticizing Co-solvents, J. Appl. Polym. Sci. 134 (23) (2017), https://doi.org/10.1002/app.44917.
[20] J.F. Snyder, R.H. Carter, E.D. Wetzel, Electrochemical and mechanical behavior in mechanically robust solid polymer electrolytes for use in multifunctional structural batteries, Chem. Mater. 19 (15) (2007) 3793–3801, https://doi.org/10.1021/cm070213o.
[21] N. Shirshova, A. Bismarck, S. Carreyette, Q.P.V. Fontana, E.S. Greenhalgh, P. Jacobsson, P. Johansson, M.J. Marczewski, G. Kalinka, A.R.J. Kucernak, J. Scheers, M.S.P. Shaffer, J.H.G. Steinke, M. Wienrich, Structural supercapacitor electrolytes based on bicontinuous ionic liquid–epoxy resin systems, J. Mater. Chem. A 1 (48) (2013) 15300–15309, https://doi.org/10.1039/C3TA13163G.
[22] N. Shirshova, H. Qian, M. Houllé, J.H.G. Steinke, A.R.J. Kucernak, Q.P.V. Fontana, E.S. Greenhalgh, A. Bismarck, M.S.P. Shaffer, Multifunctional structural energy storage composite supercapacitors, Faraday Discuss 172 (0) (2014) 81–103, https://doi.org/10.1039/C4FD00055B.
[23] S.-H. Bae, C. Jeon, S. Oh, C.-G. Kim, M. Seo, I.-K. Oh, Load-bearing supercapacitor based on bicontinuous PEO-b-P(S-Co-dvb) structural electrolyte integrated with conductive nanowire-carbon fiber electrodes, Carbon 139 (2018) 10–20, https://doi.org/10.1016/j.carbon.2018.06.039.
[24] L.D. McIntosh, M.W. Schulze, M.T. Irwin, M.A. Hillmyer, T.P. Lodge, Evolution of morphology, modulus, and conductivity in polymer electrolytes prepared via polymerization-induced phase separation, Macromolecules 48 (5) (2015) 1418–1428, https://doi.org/10.1021/ma502281k.
[25] S.A. Chopade, J.G. Au, Z. Li, P.W. Schmidt, M.A. Hillmyer, T.P. Lodge, Robust polymer electrolyte membranes with high ambient-temperature lithium-ion conductivity via polymerization-induced microphase separation, ACS Appl. Mater. Interfaces 9 (17) (2017) 14561–14565, https://doi.org/10.1021/acsami.7b02514.
[26] M.W. Schulze, L.D. McIntosh, M.A. Hillmyer, T.P. Lodge, High-modulus, high-conductivity nanostructured polymer electrolyte membranes via polymerization-induced phase separation, Nano Lett. 14 (1) (2014) 122–126, https://doi.org/10.1021/nl4034818.
[27] S.A. Chopade, S. So, M.A. Hillmyer, T.P. Lodge, Anhydrous proton conducting polymer electrolyte membranes via polymerization-induced microphase separation, ACS Appl. Mater. Interfaces 8 (9) (2016) 6200–6210, https://doi.org/10.1021/acsami.5b12366.
[28] N. Ihrner, W. Johannisson, F. Sieland, D. Zenkert, M. Johansson, Structural lithium ion battery electrolytes *via* reaction induced phase-separation, J. Mater. Chem. A 5 (48) (2017) 25652–25659, https://doi.org/10.1039/C7TA04684G.
[29] L.M. Schneider, N. Ihrner, D. Zenkert, M. Johansson, Bicontinuous electrolytes via thermally initiated polymerization for structural lithium ion batteries, ACS Appl. Energy Mater. 2 (6) (2019) 4362–4369, https://doi.org/10.1021/acsaem.9b00563.
[30] M. Cattaruzza, Y. Fang, I. Furó, G. Lindbergh, F. Liu, M. Johansson, Hybrid polymer–liquid lithium ion electrolytes: effect of porosity on the ionic and molecular mobility, J. Mater. Chem. A 11 (13) (2023) 7006–7015, https://doi.org/10.1039/D3TA00250K.
[31] S. Duan, M. Cattaruzza, V. Tu, R.M. Auenhammer, R. Jänicke, M.K.G. Johansson, F. Liu, L.E. Asp, Three-dimensional reconstruction and computational analysis of a structural battery composite electrolyte, Commun Mater 4 (1) (2023) 49, https://doi.org/10.1038/s43246-023-00377-0.
[32] E. Jacques, M. Hellqvist Kjell, D. Zenkert, G. Lindbergh, M. Behm, Expansion of carbon fibres induced by lithium intercalation for structural electrode applications, Carbon 59 (2013) 246–254, https://doi.org/10.1016/j.carbon.2013.03.015.
[33] S. Duan, A.H.S. Iyer, D. Carlstedt, F. Rittweger, A. Sharits, C. Maddox, K.-R. Riemschneider, D. Mollenhauer, M. Colliander, F. Liu, L.E. Asp, Effect of lithiation on the elastic moduli of carbon fibres, Carbon 185 (2021) 234–241, https://doi.org/10.1016/j.carbon.2021.09.037.
[34] C. Larsson, F. Larsson, J. Xu, K. Runesson, L.E. Asp, Effects of lithium insertion induced swelling of a structural battery negative electrode, Compos. Sci. Technol. 244 (2023) 110299, https://doi.org/10.1016/j.compscitech.2023.110299.
[35] L.E. Asp, K. Bouton, D. Carlstedt, S. Duan, R. Harnden, W. Johannisson, M. Johansen, M.K.G. Johansson, G. Lindbergh, F. Liu, K. Peuvot, L.M. Schneider, J. Xu, D. Zenkert, A structural battery and its multifunctional performance, Adv Energy Sustain Res 2 (3) (2021) 2000093, https://doi.org/10.1002/aesr.202000093.
[36] K. Muniandy, Z. Mohamad Ariff, A. Abu Bakar, Digital image correlation utilization in measuring displacement and strain during plastic film blowing process: a feasibility study, Measurement 136 (2019) 487–500, https://doi.org/10.1016/j.measurement.2018.12.093.
[37] M.S. Siraj, S. Tasneem, D. Carlstedt, S. Duan, M. Johansen, C. Larsson, J. Xu, F. Liu, F. Edgren, L.E. Asp, Advancing Structural Battery Composites: Robust Manufacturing for Enhanced and Consistent Multifunctional Performance, Adv Ener Sust Res n/a (2024) 2300109, https://doi.org/10.1002/aesr.202300109.
[38] M.S. Hong, I.J. Chung, The cure behavior of vinyl ester resin with low profile additive I. Cure kinetics and TTT cure diagram, Polym. J. 23 (6) (1991) 747–755, https://doi.org/10.1295/polymj.23.747.
[39] L.E. Asp, L.A. Berglund, R. Talreja, A criterion for crack initiation in glassy polymers subjected to a composite-like stress state, Compos. Sci. Technol. 56 (11) (1996) 1291–1301, https://doi.org/10.1016/S0266-3538(96)00090-5.
[40] N. J. Saleh, A. A. Abdul Razak, M. A. Tooma, M.A. E. Aziz, Study mechanical properties of epoxy resin cured at constant curing time and temperature with different hardeners, Eng. Technol. J. 29 (9) (2011) 1804–1819, https://doi.org/10.30684/etj.29.9.15.
[41] G. Sines, M. Adams, Compression testing of ceramics, in: R.C. Bradt, D.P. H. Hasselman, F.F. Lange (Eds.), Flaws and Testing, Fracture Mechanics of Ceramics, Springer US, Boston, MA, 1978, pp. 403–434, https://doi.org/10.1007/978-1-4615-7017-2_23.